Loss of Corneal Epithelial Heparan Sulfate Leads to Corneal Degeneration and Impaired Wound Healing

Vivien Jane Coulson-Thomas,*[,1] Shao-Hsuan Chang,[1] Lung-Kun Yeh,[2] Yvette May Coulson-Thomas,[3] Yu Yamaguchi,[4] Jeffrey Esko,[5] Chia-Yang Liu,[1] and Winston Kao[1]

[1]Department of Ophthalmology, University of Cincinnati, Cincinnati, Ohio, United States
[2]Department of Ophthalmology, Chang-Gung Memorial Hospital, Chang-Gung University College of Medicine, Linko, Taiwan
[3]Department of Biochemistry, Universidade Federal de São Paulo, São Paulo, São Paulo, Brazil
[4]Sanford Children's Health Research Center, Sanford-Burnham Medical Research Institute, La Jolla, California, United States
[5]Department of Cellular and Molecular Medicine, Glycobiology Research and Training Center, University of California-San Diego, La Jolla, California, United States

Correspondence: Vivien Jane Coulson-Thomas, John van Geest Centre for Brain Repair, Robinson Way, Cambridge CB2 0PY, UK; vcoulsonthomas@gmail.com, vc315@cam.ac.uk.

Current affiliation: *John van Geest Centre for Brain Repair, University of Cambridge, Cambridge, United Kingdom.

Submitted: July 28, 2014
Accepted: April 5, 2015

Citation: Coulson-Thomas VJ, Chang S-H, Yeh L-K, et al. Loss of corneal epithelial heparan sulfate leads to corneal degeneration and impaired wound healing. *Invest Ophthalmol Vis Sci*. 2015;56:3004–3014. DOI:10.1167/iovs.14-15341

Purpose. Heparan sulfate (HS) is a highly modified glycosaminoglycan (GAG) bound to a core protein to form heparan sulfate proteoglycans (HSPGs) that are vital in many cellular processes ranging from development to adult physiology, as well as in disease, through interactions with various protein ligands. This study aimed to elucidate the role of HS in corneal epithelial homeostasis and wound healing.

Methods. An inducible quadruple transgenic mouse model was generated to excise *Ext1* and *Ndst1*, which encode the critical HS chain elongation enzyme and *N*-deacetylase/*N*-sulfotransferase, respectively, in keratin 14-positive cells upon doxycycline induction.

Results. $EXT^{\Delta/\Delta CEpi}$ mice (deletion of *Ext1* in corneal epithelium) induced at P20 presented progressive thinning of the corneal epithelium with a significant loss in the number of epithelial layers by P55. $EXT^{\Delta/\Delta CEpi}$ mice presented tight junction disruption, loss of cell–basement membrane adhesion complexes, and impaired wound healing. Interestingly, $EXT^{\Delta/\Delta CEpi}$ and $NDST^{\Delta/\Delta CEpi}$ mice presented an increase in cell proliferation, which was assayed by both Ki67 staining and 5-ethynyl-2′-deoxyuridine (EdU) incorporation. Moreover, $EXT^{\Delta/\Delta CEpi}$ mice presented compromised epithelial stratification 7 days after a debridement wound. The conditional knockout of HS from keratocytes using the keratocan promoter led to no corneal abnormalities or any disruption in wound healing.

Conclusions. Corneal epithelial cells require HS for maintaining corneal homeostasis, and the loss of epithelial HS leads to both impaired wound healing and impaired corneal stratification.

Keywords: heparan sulfate, syndecan-1, syndecan-4, corneal epithelium, corneal stratification

Heparan sulfate (HS) is highly modified glycosaminoglycan (GAG) bound to a core protein to form heparan sulfate proteoglycans (HSPGs). Heparan sulfate proteoglycans are vital in many cellular processes ranging from development to adult physiology, as well as in disease, through interactions with various protein ligands. The fine structure of HS is characterized by specific modification patterns that are cell specific, age specific, and organism dependent.[1] The fine structure of the sugar chains modulates the activity of HSPGs. The biosynthesis of HS commences with the addition of a linkage tetrasaccharide that is attached to a serine residue of a proteoglycan core protein. A xylose residue is first added by xylosyl transferase, and thereafter three different enzymes add the remaining –galactose–galactose–glucuronic acid. The addition of a N-acetylglucosamine commits the GAG to a HS/heparin (HEP), generated by the polymerase complex composed of exostosin glycosyltransferase 1 (*Ext1*) and exostosin glycosyltransferase 2 (*Ext2*), which add alternating units of glucuronic acid and N-acetylglucosamine to the nonreducing end of the chain. After this polymerization step, a set of modifications occurs: N-deacetylation/N-sulfation of N-acetyl-glucosamine by a bifunctional enzyme, glucosaminyl *N*-deacetylase/*N*-sulfotransferase (*Ndst*); epimerization of the glucuronic acid adjacent to the recently N-sulfated domain by C5-glucuronosyl epimerase; and 2-, 3-, and 6-O sulfation by different sulfotransferases with specific tissue distribution and isoforms. These modifications to the HS chain generate variable specific epitopes along the GAG chain with specific sulfation patterns.

Heparan sulfate proteoglycans are found on the cell surface and in the extracellular matrix (ECM) where they influence a variety of biological processes by interacting with physiologically important proteins, such as growth factors, chemokines and cytokines, ECM proteins, enzymes, and enzyme inhibitors.[2] Their activity is due in a large part to the pattern of sulfated sugar residues along the HS chains covalently bound to the core proteins of the proteoglycans.[3–6] The interaction of growth factors with HS protects the growth factors from degradation, creates a storage pool, acts as a coreceptor facilitating the assembly of signaling complexes, regulates growth factor diffusion throughout the tissue, and enables clearance of the growth factors by endocytosis.[2,7,8] Heparan sulfate proteoglycans are ubiquitously expressed and can be found on the cell surface (syndecan-1, -2, -3, and -4 or glypican-1, -2, -3, -4, -5, and -6) and in the ECM (perlecan).

The cornea is a specialized tissue that attains the ability to remain transparent and serves as the major refractive tissue to cast images onto the retina for vision. The ability to remain transparent requires healthy functioning of all corneal components, namely, the endothelium, epithelium, and stroma, working in synergy. Any perturbation and/or damage to the endothelium, stroma, or epithelium can lead to corneal haze. Upon corneal insults, such as corneal wounding, the healing process must occur in an efficient manner, thereby avoiding an exacerbated inflammatory response that could lead to angiogenesis and compromise the regeneration of corneal transparency. The healing of corneal epithelial wounds begins with the migration of an epithelial sheet at the wound edge to resurface the defect.[9–11] Thereafter, there is an increase in epithelial cell proliferation away from the wound edge and in the limbal region.[12] Numerous growth factors, cytokines, morphogens, and ECM proteins, derived from either the epithelium or the underlying stromal layer, have been implicated in the regulation of epithelial cell migration and proliferation during corneal repair.[10,12,13] Failure to re-epithelialize efficiently may lead to infection and/or persistent corneal wounds. Therefore, it is of vital importance to understand the steps involved in the wound healing process, which would provide the basic understanding necessary to develop strategies for promoting wound healing.

To date, limited research has been directed toward the study of HS and HSPGs in the cornea. The few studies available investigated primarily the role of individual HSPGs, more precisely syndecan-1 and perlecan, and the role of sulfatases 1 and 2 (Sulf 1 and 2) in corneal wound healing. Currently, corneal research on proteoglycans has focused primarily on chondroitin sulfate proteoglycans, keratan sulfate proteoglycans, and more specifically the small leucine-rich proteoglycans. Therefore, this study aimed to elucidate the role of HS in corneal homeostasis and wound healing. To that end, HS was knocked out of corneal compartments using specific site-directed and inducible excision of *Ext1* and *Ndst1*. *Ext1* and *Ndst1* were knocked out of cells of epithelial origin using a Krt14-rtTA driver system generating $EXT^{\Delta/\Delta CEpi}$ mice (excision of *Ext1* in stratified corneal epithelium) and $NDST^{\Delta/\Delta CEpi}$ mice (excision of *Ndst1* in corneal stratified epithelium). Therefore, with the Krt14-driven knockout system, HS was specifically ablated from the basal cells of the corneal epithelium. Heparan sulfate was also knocked out of corneal stromal keratocytes using the keratocan driver mouse generating $EXT^{\Delta/\Delta CStr}$ mice (*Kera-Cre/Ext1*$^{f/f}$, deletion of *Ext1* in corneal stromal keratocytes). Our findings reveal the vital role that HS plays in corneal epithelial homeostasis and in corneal epithelial wound healing. Heparan sulfate is required for the maintenance of tight junctions, which is essential for the protective/barrier function of the corneal epithelium. The loss of HS impedes wound healing after epithelium debridement, and the severity of the phenotype is a testament to the importance of HS in corneal homeostasis.

Materials and Methods

Mouse Strains and Genotyping

Transgenic mouse lines Krt14-rtTA (stock number 008099),[14] tet-O-Cre (TC) (stock number 006224),[15] and RosamTmG/mTmG (stock number 007576)[16] were purchased from the Jackson Laboratory (Bar Harbor, ME, USA). The floxed mice used were *Ext1*$^{f/f}$[17] and *Ndst1*$^{f/f}$.[18] Compound transgenic mice were generated by mating. The identification of each transgene allele was performed by PCR genotyping with tail DNA. All the mice were bred at the Animal Facility of the University of Cincinnati Medical Center. Animal care and use conformed to the ARVO Statement for the Use of Animals in Ophthalmic and Vision Research. All animal protocols were approved by the Institutional Animal Care and Use Committee (IACUC) of the University of Cincinnati.

Induction by Administration of Doxycycline Chow

Administration of Dox-chow was used to induce Krt14-driven persistent and irreversible excision of *Ext1* or *Ndst1* in tetratransgenic mice (*Krt14-rtTA/TC/RosaLSL/Ext1*$^{f/f}$ or *Krt14-rtTA/TC/RosaLSL/Ndst1*$^{f/f}$). Transgenic mice at postnatal day 20 (P20) or older were fed with Dox-chow (doxycycline 1 g/kg chow; Custom Animal Diets, LLC, Bangor, PA, USA) ad libitum. Control animals were either double transgenic or triple transgenic heterozygous littermates.

Eyeball Collection

Eyeballs were obtained from $EXT^{\Delta/\Delta CEpi}$ and $NDST^{\Delta/\Delta CEpi}$ mice and littermate control mice and fixed in 2% paraformaldehyde for paraffin embedding, cryosectioning, and whole-mount analysis, and in 0.1 M cacodylate buffer (pH 7.4) containing 2% glutaraldehyde and 2% paraformaldehyde for electron microscopy.

Debridement Wound

Debridement wounds were performed as previously described.[12] Briefly, mice were anesthetized by intraperitoneal injection of ketamine hydrochloride (5 mg/g body weight) and xylazine (0.625 mg/g body weight). The corneal wound area was demarcated with a 1.5-mm-diameter biopsy punch, and the epithelial debridement wound was performed with an AlgerBrush (Alger Company, Inc., Lago Vista, TX, USA). Thereafter, the loose cells were removed by washing with PBS and a sponge swab.

Quantification of HS Content in the Corneal Epithelium

The corneal epithelium was removed from five mice under a stereomicroscope with the use of both an AlgerBrush (Alger Company) and a blade and then pooled. The epithelium was washed in acetone, followed by centrifugation and removal of excess acetone. The pellet was left to dry, suspended in chondroitinase ABC (C3667; Sigma-Aldrich Corp., St. Louis, MO, USA), and left for 24 hours at 37°C. Thereafter, the digested products were removed using centrifugal filter units (Microcon 3000, 500 μL; Millipore, Billerica, MA, USA). Heparan sulfate was then analyzed using the carbazole reaction. Briefly, 150 μL 0.025 M sodium tetraborate prepared in sulfuric acid and 50 μL 0.125% carbazole in absolute ethanol (wt/vol) were added to 20 μL of each sample or standard curve in a 96-well microplate and placed in an incubator (hot air oven) set at 100°C for 10 minutes. The plate was removed and left to cool on ice for 2 minutes, then placed on a plate mixer; the absorbance was measured at 530 nm using a Victor II (Perkin Elmer, Waltham, MA, USA).

EdU Labeling

Cell proliferation was determined by EdU (5-ethynyl-2′-deoxyuridine; Life Technologies, Eugene, OR, USA) incorporation. Mice were labeled with 100 μg EdU/g body weight by intraperitoneal injection for 4 hours following a debridement wound. Unwounded littermate control mice also received EdU injections, providing proliferation control sections. Thereafter,

Investigative Ophthalmology & Visual Science

the mice were killed by CO_2 inhalation and their eyeballs enucleated, fixed in 2% buffered paraformaldehyde, and treated for 15 minutes in 0.1% sodium borohydrate. The tissues were then embedded in Tissue-Tek embedding medium (Sakura Finetek USA, Inc., Torrance, CA, USA) for cryosectioning. Sections (10 μm) were cut using a CryoStar NX70 (Thermo Scientific, Waltham, MA, USA) cryostat and collected on Fisherbrand SuperfrostPlus Gold microscope slides (Thermo Scientific). Upon use, sections were incubated for 30 minutes at 37°C, and excess tissue embedding medium was removed with PBS. Unspecific protein binding sites were blocked with 5% fetal bovine serum (FBS). The incorporated EdU was developed using the Click-IT Alexa Fluor 647 kit (Life Technologies) to reveal the incorporated EdU. The nuclei were counterstained with DAPI. Images were captured using a Zeiss Observer Z1 inverted microscope or Zeiss LSM-710 confocal microscope and images analyzed using the Zeiss LSM Image Browser 3.2 software (Zeiss, Oberkochen, Germany).

Transmission Electron Microscopy

Cornea samples were obtained and fixed in 0.1 M cacodylate buffer (pH 7.4) containing 2% glutaraldehyde and 2% paraformaldehyde for 2 hours at 4°C and then preserved overnight in 0.1 M cacodylate buffer (pH 7.4) containing 2% glutaraldehyde at 4°C. After refixation in 1% osmium tetroxide (OsO_4) for 1 hour at 48°C, cornea samples were washed in 0.1 M cacodylate buffer (pH 7.4) three times for 10 minutes each, then dehydrated in a graded ethanol series and embedded in Epon 812 epoxy resin (Polysciences, Inc., Warrington, PA, USA). Ultrathin 50-nm sections were stained with uranyl acetate and lead citrate, and images were photographed with a Hitachi 7500 transmission electron microscope (Hitachi, Tokyo, Japan) equipped with an AMT digital camera.

Immunohistochemistry

Tissues were fixed for 30 minutes in 2% buffered paraformaldehyde, washed five times with PBS, sequentially dehydrated, immersed in paraffin overnight, and subsequently mounted. The blocks were sectioned at 6 μm and the sections collected on poly-L-lysine-treated slides. Upon use, the paraffin sections were washed with xylene to remove excess paraffin and then rehydrated. Unspecific protein binding sites were blocked with 5% FBS and endogenous peroxidase activity quenched with 3% hydrogen peroxide. Sections were then incubated with the primary antibodies anti-Krt14 (PRB-155P; Covance, Princeton, NJ, USA), anti-Krt12 produced at the University of Cincinnati,[19,20] anti-syndecan-1 (ab34164; Abcam, Cambridge, MA, USA), anti-syndecan-2 (ab79978; Abcam), anti-syndecan-3 (ab63932; Abcam), anti-syndecan-4 (ab24511; Abcam), and anti-fibronectin (AB2033; Millipore). Sections were washed and incubated with appropriate secondary antibodies produced in donkey conjugated with biotin for 1 hour at 18°C. Thereafter, the tissues were developed using the Pierce Peroxidase IHC Detection Kit (Thermo Scientific). Sections were mounted and images were captured of solely diaminobenzidine (DAB) staining using a Nikon Eclipse E800 microscope (Tokyo, Japan) coupled to a Zeiss AxioCam ICc5 camera, and images were analyzed using AxioVision (Zeiss). Secondary control was carried out with goat IgG isotype control (ab37388; Abcam) in place of the primary antibody and did not yield any DAB staining (results not shown). Subsequently the sections were washed and counterstained with hematoxylin. Sections were dehydrated and mounted in Permount (Electron Microscopy Sciences, Hatfield, PA, USA). Images were also captured with hematoxylin counterstain using a Nikon Eclipse E800 microscope coupled to a Zeiss AxioCam ICc5 camera and images analyzed using AxioVision (Zeiss).

Immunofluorescence

For immunofluorescence analysis, eyeballs were fixed for 30 minutes in 2% buffered paraformaldehyde and treated for 15 minutes in 0.1% sodium borohydrate. Thereafter, the tissues were embedded in Tissue-Tek (Sakura Finetek USA, Inc.) embedding medium for cryosectioning. Sections (10 μm) were cut using a Cryostar NX70 (Thermo Scientific) cryostat and collected on Fisherbrand SuperfrostPlus Gold microscope slides (Thermo Scientific). Upon use, sections were incubated for 30 minutes at 37°C and excess tissue embedding medium was removed with PBS. Unspecific protein binding sites were blocked with 5% FBS. Sections were stained with anti-HS (clone 10E4; US Biological, Salem, MA, USA), anti-ZO-1 (40-2200; Invitrogen, Carlsbad, CA, USA), and anti-E cadherin (610181; BD Transduction Lab, Franklin Lakes, NJ, USA) followed by donkey anti-mouse 488 (Life Technologies) and donkey anti-rabbit 555 (Life Technologies). The nucleus was counterstained with DAPI. Images were captured using a Zeiss Observer Z1 inverted microscope or Zeiss LSM-710 confocal microscope, and images were analyzed using the LSM Image Browser 3.2 software (Zeiss).

Whole-Mount Analysis

Corneas were excised from enucleated eyeballs, treated for 15 minutes in 0.1% sodium borohydrate and unspecific protein binding sites blocked with 5% FBS for 24 hours with shaking. The corneas were then incubated with the primary antibody rabbit anti-Krt12 or anti-Ki67 (Abcam, ab15580) for 24 hours followed by the secondary antibody, donkey anti-rabbit Alexa Fluor 647 (Life Technologies). Nuclei were counterstained with DAPI. Corneas were mounted in Fluoromount-G (Electron Microscopy Sciences). Images were captured using a Zeiss Observer Z1 inverted microscope or Zeiss LSM-710 confocal microscope, and the images were analyzed using the LSM Image Browser 3.2 software (Zeiss).

Fluorescein Staining

A drop of Flura-Safe Fluorexon Disodium & Benoxinate Hydrochloride Ophthalmic Solution 0.35%/0.4% (Apollo Ophthalmics, Newport Beach, CA, USA) was placed over the murine eyeball and left for 1 minute. Thereafter any excess was removed with PBS washes and a sponge swab. The experiment was carried out on five mice for each experimental group and repeated twice, resulting in 10 animals per group.

Statistics

All values are presented as means ± standard deviation of the mean. The difference between two groups was compared by Student's *t*-test. $P < 0.05$ was considered statistically significant. Statistical analysis was performed with the GraphPad Prism version 5 software package (GraphPad Software, San Diego, CA, USA).

Results

Ext1 Excision From the Corneal Epithelium

Quadruple and triple transgenic mice *Krt14-rtTA/tet-O-cre/Ext1^{flox}/mTmG* and *Krt14-rtTA/tet-O-cre/Ndst1^{flox}* were generated to specifically excise *Ext1* and *Ndst1*, respectively, upon Dox induction in keratin 14-expressing cells; hence, HS

Investigative Ophthalmology & Visual Science

or HS downstream modifications were not expressed in the stratified corneal epithelium (CEpi)-generating *EXT*$^{\Delta/\Delta CEpi}$ and *NDST*$^{\Delta/\Delta CEpi}$ mice. Prior to Dox induction, the *K14-rtTA/tet-O-cre/Ext1*^{flox}*/mTmG* and *K14-rtTA/tet-O-cre/Ndst1*^{flox} mice exhibited no corneal or eye abnormalities.

Keratin 14 (Krt14) staining has previously been demonstrated to be expressed by the basal cells of the corneal epithelium, and therefore *Ext1* and *Ndst1* were ablated from the basal cells of the corneal epithelium upon doxycycline induction.[21,22] The stratified corneal epithelium is composed of a layer of columnar basal cells in contact with the basement membrane and thereafter the suprabasal and superficial layers. The suprabasal and superficial layers are dependent on cell–cell adhesion molecules to maintain structural integrity. The suprabasal epithelial cells (also known as wing cells) are cuboidal, while the superficial cell layers are flattened (squamous). The basal epithelial cells divide vertically to yield a daughter cell that remains attached to the underlying basement membrane and another daughter cell that moves upward to replenish the superficial cells that slough off, thereby maintaining corneal epithelial homeostasis. The suprabasal cells are derived from the basal epithelial cells and give rise to the remaining epithelium, and the turnover of such cells is approximately 2 weeks.[23]

The *EXT*$^{\Delta/\Delta CEpi}$ mice were bred with the reporter *mTmG* gene, which expresses strong red fluorescence in all tissues; however, in cells expressing Cre recombinase, the *mT* cassette is deleted, enabling the expression of the downstream cassette, membrane-targeted enhanced GFP (*mG*). Therefore, *EXT*$^{\Delta/\Delta CEpi}$ mice would express the *mT* cassette in the endothelial cells and keratocytes; however, in the epithelial cells, which present K14-driven Cre recombinase activity, both the floxed *Ext1* gene and *mT* cassette would be deleted, and cells will consequently express membrane-bound GFP (Fig. 1). Figure 1 shows a z-stack of images obtained from *EXT*$^{\Delta/\Delta CEpi}$ mouse central cornea. Confocal microscopy was used to verify that the cells of the anterior cornea express the desired markers. An image from the central stroma is displayed in the center of the figure, and the depth of this image is represented with a blue line in the z-stack projection at the top and to the right of the figure. The z-stack projections (shown at the top and to the right of the figure) represent a cut view through the cornea enabling visualization of the corneal epithelium in green (expressing *mG*) and of the stroma and endothelium in red (due to the absence of Cre recombinase activity, which deletes the *mT* cassette). The precise location of the z-stack projection presented at the top of the figure (with a green border) is indicated by a green line in the central image; and similarly, the location of the z-stack projection to the right is represented by a red line in the figure.

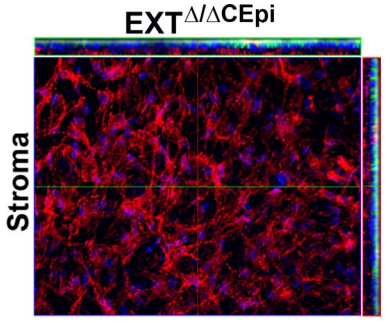

Figure 1. *mTmG* expression in *EXT*$^{\Delta/\Delta CEpi}$ corneal whole mount. Mice were bred with the reporter *RosamTmG* gene whereby K14-positive cells, which express Cre recombinase upon induction, express membrane-targeted enhanced green fluorescent protein (EGFP; *mG*) representing *Ext1*-deficient cells in *EXT*$^{\Delta/\Delta CEpi}$ mice. A series of images was collected to cover the whole stromal thickness as a continuous z-axis scan through the entire corneal stroma starting from the superficial layer of the corneal epithelium and ending at the corneal endothelium and presented as a three-dimensional image. The corneal epithelium is represented in *green* by *mG* expression, and the corneal stroma and endothelium are represented in *red* by *mT* expression. A representative image of the corneal stroma is shown, indicating the absence of Cre recombinase activity in the stroma. Nuclei were stained with DAPI (*blue*).

Role of HS in the Structural Integrity of the Corneal Epithelium

Corneas of mice induced from P21 to P35, P21 to P55, and P21 to P120 were analyzed by electron microscopy in order to evaluate the structural integrity of the stratified epithelium (Figs. 2A–C, respectively). There was no difference in the overall number of cell layers in *EXT*$^{\Delta/\Delta CEpi}$ mice induced from P21 to P35; however, they presented a decrease in the number of cuboidal cell layers (suprabasal and wing cells) and an increase in the number of squamous cell layers (Fig. 2A). *EXT*$^{\Delta/\Delta CEpi}$ mice induced from P21 to P55 and P21 to P120 both presented an overall reduction in the number of cell layers, from approximately 10 layers in the littermate control mice to approximately five and three layers, respectively (Figs. 2B, 2C; Supplementary Fig. S1). *EXT*$^{\Delta/\Delta CEpi}$ mice induced from P21 to P55 presented an overall loss of columnar suprabasal epithelial cells and wing cells with a tendency toward one or two layers of basal or suprabasal cuboidal epithelial cells (Fig. 2B). *EXT*$^{\Delta/\Delta CEpi}$ mice induced from P21 to P120 presented a drastic loss of corneal structural integrity and a very thin corneal epithelium (Fig. 2C). There was a loss of wing, columnar basal, cuboidal suprabasal, and stratified epithelial cells (Figs. 2C[b], 2C[c]). Therefore, the loss of HS could compromise adhesion junctions between the basal epithelial cells and the basement membrane and also adhesion complexes between epithelial cells, leading to a loss of epithelial cell morphology and a reduced number of cell layers. Interestingly, our previous work showed that there is skin epithelial hyperplasia in *EXT1*$^{\Delta/\Delta StrEpi}$ (deletion of *Ext1* in stratified epidermal epithelium) mice, which present thick dense skin epithelium.[24]

Differentiation of Stratified Epithelium

In adult mice (older than 3 months), most of the basal corneal epithelial cells express Krt14 and Krt12 simultaneously, while the suprabasal and superficial cells express only Krt12 and not Krt14. Therefore, Krt12 has been recognized as a marker of corneal epithelium differentiation. Interestingly, there was a loss of Krt12 expression in the epithelial cells of *EXT*$^{\Delta/\Delta CEpi}$ mice induced from both P21 to P55 (Fig. 3) and P21 to P120 (results not shown). The whole-mount images were of the cell layer immediately adjacent to the basal cells (second cell layer, as represented in Supplementary Fig. S2), representing the suprabasal cell layer in *EXT*$^{f/f}$. *EXT*$^{\Delta/\Delta CEpi}$ mice presented weak K12 staining solely in the superficial layer of the stratified epithelial cells (Fig. 3). The lack of K12 staining in *EXT*$^{\Delta/\Delta CEpi}$ mice further indicates a loss of the epithelial suprabasal layer and wing cells. These results suggest that the loss of HS could impair proper stratification and differentiation of corneal epithelial cells or that the epithelium could be forced to regenerate at a fast rate because of excessive sloughing off of epithelial cells due to impaired cell–cell adhesion, thereby compromising differentiation of the epithelial cells.

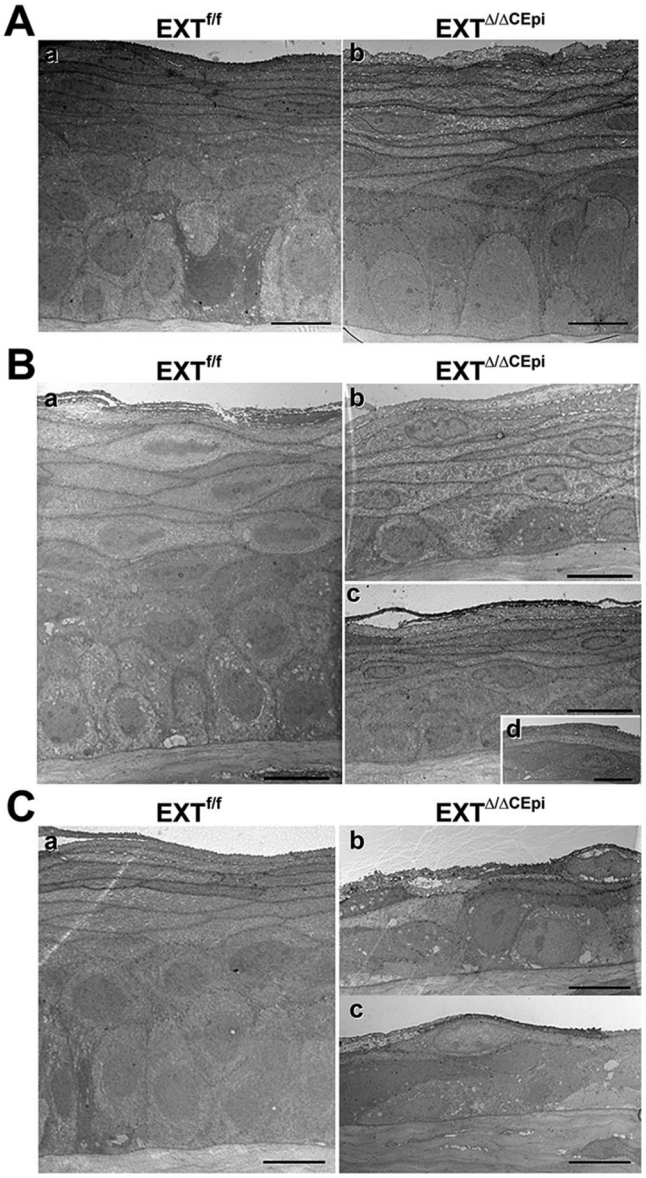

Figure 2. Electron microscopy images of stratified epithelium. Corneas from $EXT^{f/f}$ (**Aa**, **Ba**, **Ca**) and $EXT^{\Delta/\Delta CEpi}$ mice (**Ab**, **Bb–Bd**, **Cb**, **Cc**) were collected at P35 (**A**), P55 (**B**), and P120 (**C**). Mice were induced at P21. $EXT^{\Delta/\Delta CEpi}$ mice present compromised stratified epithelium and loss of cell layers in a time-dependent manner. *Scale bars*: 10 μm.

Analysis of Tight Junctions in Corneal Stratified Epithelium of $EXT^{\Delta/\Delta CEpi}$ Mice

In order to evaluate whether the loss of HS in corneal epithelial cells affects cell–cell tight junctions, the corneas of live mice were treated with 0.25% fluorescein solution for 1 minute and subsequently rinsed with PBS. Fluorescein solution does not penetrate healthy corneas due to the presence of tight junctions between the corneal epithelial cells; however, upon wounding or loss of tight junctions between cells, the fluorescein solution penetrates the area with the corneal defect. Interestingly, the $EXT^{\Delta/\Delta CEpi}$ mice induced from both P21 to P55 (Figs. 4b, 4e) and P21 to P120 (Figs. 4c, 4f) presented corneas with dense fluorescein staining without prior wounding. The cell–cell boundaries are evidenced by fluorescein staining, suggesting that fluorescein is penetrating the corneas through impaired cell–cell adhesion. These results therefore suggest that the epithelium could undergo excessive sloughing off of epithelial cells due to impaired cell–cell adhesion.

E-cadherin staining further demonstrated a loss of cell–cell tight junctions in $EXT^{\Delta/\Delta CEpi}$ mice when compared to the littermate control (Fig. 5A). ZO-1 staining in the littermate control mice revealed the cell–cell tight junctions and also the cell–basement membrane adhesion complexes (Figs. 5A, 5B). In $EXT^{\Delta/\Delta CEpi}$ mice there was a loss of ZO-1 staining between the basal cell layer and basement membrane, suggesting a loss of cell–basement membrane adhesion complexes (Fig. 5A, arrowheads). $EXT^{\Delta/\Delta CEpi}$ mice also presented a loss of ZO-1 staining between epithelial cells demonstrating compromised cell–cell junctions (Figs. 5A, 5B). Thus, ZO-1 and E-cadherin staining further evidenced the compromised cell–cell and cell–basement membrane adhesion complexes in $EXT^{\Delta/\Delta CEpi}$ mice, which could account for an increase in sloughing off of epithelial cells.

Reduction in the Number of Cell Layers in $EXT^{\Delta/\Delta CEpi}$ Mice

Corneas isolated from $EXT^{\Delta/\Delta CEpi}$ mice induced from P21 to P55 were subjected to paraffin embedding and sectioning. Hematoxylin and eosin (H&E) staining further evidenced the drastic reduction in the number of cell layers shown by electron microscopy (Figs. 6A–C). In order to investigate whether $EXT^{\Delta/\Delta CEpi}$ mice present impaired wound healing, mice were subjected to debridement and analyzed after 24 hours (Fig. 6A). Within 24 hours, the epithelial cells were able to cover the wound area and initiate stratification in littermate control mice; however, full stratification was not complete at 24 hours (Figs. 6B, 6C). On the other hand, 70% of the wound area persisted in $EXT^{\Delta/\Delta CEpi}$ mice 24 hours after wounding (Fig. 6D). Analysis of the area showing resurfaced epithelium in $EXT1^{\Delta/\Delta CEpi}$ mice revealed the absence of a stratified epithelium, presenting solely a single cell layer in the resurfaced area (Figs. 6A–C). In order to evaluate the efficiency of the *Ext1* ablation, HS immunostaining was performed with anti-HS (clone 10E4; US Biological), revealing the absence of HS in $EXT^{\Delta/\Delta CEpi}$ murine corneas (Fig. 6C). The loss of HS was further confirmed by quantifying HS extracted from the corneal epithelium, demonstrating an ~80% reduction in HS content (Fig. 6E).

Syndecan Expression During Corneal Wound Healing

In order to evaluate the expression pattern of HSPGs in the corneas of $EXT^{\Delta/\Delta CEpi}$ mice, immunostaining was performed for syndecan-1, -2, -3, and -4. Strong staining for syndecan-1 and -4 was detected primarily in the basal cells of the corneal epithelium of the littermate control mice (Figs. 7A–D, respectively, top left). In the corneas of the littermate control mice 24 hours after wounding, dense syndecan-1 and -4 expression was no longer restricted to the basal and suprabasal cells and was present throughout the epithelium, which is not yet a mature stratified epithelium (Figs. 7A–D, bottom left). There was significantly less syndecan-1 staining in the corneal epithelium of $EXT^{\Delta/\Delta CEpi}$ mice, in both wounded and unwounded corneas (Figs. 7A, 7C, right). On the other hand, there was significantly less syndecan-4 expression solely in the wounded corneas when compared to the unwounded corneas (Figs. 7B, 7D, right). The change in syndecan-1 and -4 distribution in $EXT^{\Delta/\Delta CEpi}$ mice can be seen in the absence of H&E staining (Figs. 7C, 7D). No significant staining was observed for syndecan-2 and -3 (results not shown).

Investigative Ophthalmology & Visual Science

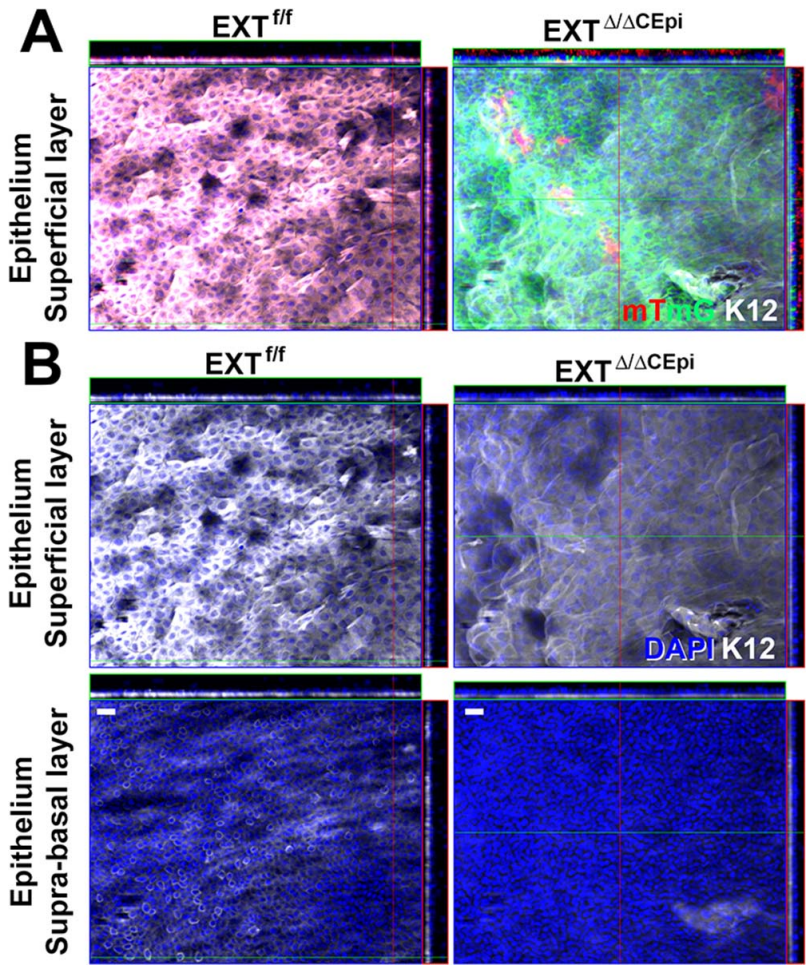

Figure 3. Krt12 staining of corneal whole mounts. Corneas isolated from $EXT^{f/f}$ and $EXT^{\Delta/\Delta CEpi}$ mice at P55 were analyzed by whole-mount immunostaining. (**A**) Krt12 (*white*) staining was colocalized with *mTmG* representing the cells from which *Ext1* was ablated (*green*), revealing a loss of Krt12 staining in *Ext1*-null cells. (**B**) Krt12 (*white*) staining in the suprabasal and superficial layers of the cornea. $EXT^{\Delta/\Delta CEpi}$ mice present a loss of Krt12 staining in the suprabasal and wing cell layers and a decrease in the superficial layer of the cornea. *Scale bars*: 20 μm.

Fibronectin is a glycoprotein present in the corneal basement membrane to which integrins and syndecans on the basolateral regions of the basal epithelial cells bind, forming adhesion complexes. Fibronectin and syndecan interactions play a fundamental role in epithelial cell adhesion and migration. Fibronectin is upregulated in the littermate corneas 24 hours after wounding (Supplementary Fig. S2, left). $EXT^{\Delta/\Delta CEpi}$ mice present significantly less fibronectin when compared to littermate controls and fail to upregulate fibronectin after wounding (Supplementary Fig. S2, right).

Knockout of HS Impairs Stratification of the Corneal Epithelium After Wounding

In order to verify whether $EXT^{\Delta/\Delta CEpi}$ epithelial cells are able to stratify after corneal debridement wounds, the corneas were wounded and left for 7 days to enable the formation of a mature stratified epithelium (Fig. 8). Indeed, the littermate control mice presented a stratified epithelium similar to that of the unwounded mice; however, $EXT^{\Delta/\Delta CEpi}$ mice were unable to form a stratified epithelium within 7 days after wounding (Fig. 8, bottom right). Moreover, $EXT^{\Delta/\Delta CEpi}$ mice still presented a single epithelial cell layer, suggesting that HS is essential for successful stratification of the corneal epithelium (Fig. 8).

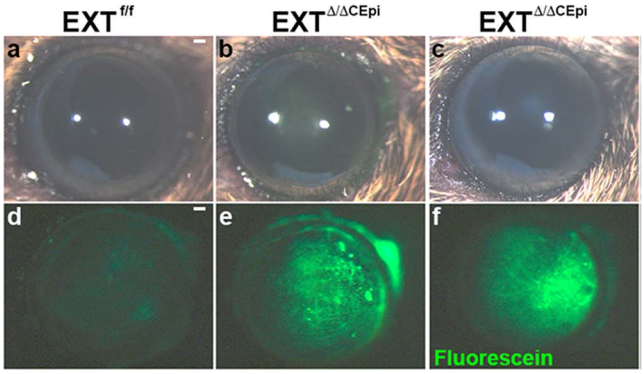

Figure 4. Loss of barrier function in $EXT^{\Delta/\Delta CEpi}$ mice. Images were captured of $EXT^{f/f}$ (**a**) and $EXT^{\Delta/\Delta CEpi}$ mice (**b**, **c**) induced from P21 to P55 and P21 to P120, respectively) prior to fluorescein administration using a stereomicroscope coupled with white light. Fluorescein sodium 0.25% was applied as an eye drop to the eyes of P55 $EXT^{f/f}$ (**d**) mice, $EXT1^{\Delta/\Delta CEpi}$ (**e**) mice induced from P21 to P55, and $EXT^{\Delta/\Delta CEpi}$ (**f**) mice induced from P21 to P120. Excess fluorescein was washed off with PBS and images were acquired using the 488 filter set. *Scale bar*: 250 μm.

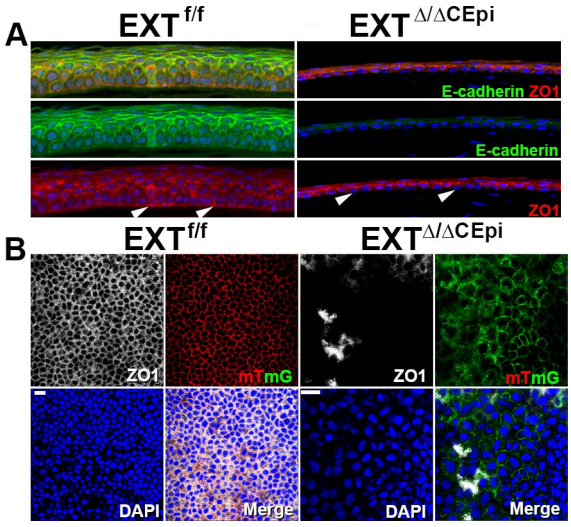

Figure 5. Loss of cell–cell and cell–basement membrane tight junctions in *EXT*$^{\Delta/\Delta CEpi}$ mice. (**A**) ZO-1 (*red*) and E-cadherin (*green*) staining was analyzed in sections of *EXT*$^{f/f}$ and *EXT*$^{\Delta/\Delta CEpi}$ mice induced from P21 to P55. ZO-1 staining evidences the loss of adhesion complexes between the basal epithelial cells and basement membrane (*arrowheads*). (**B**) Whole-mount analysis was performed to analyze ZO-1 (*white*) distribution throughout the cornea of *EXT*$^{f/f}$ and *EXT*$^{\Delta/\Delta CEpi}$ mice induced from P21 to P55. Corneas used for whole-mount analysis contained the *mTmG* gene whereby cells lacking *Ext1* present membrane-bound GFP (*green*), whereas the corneal epithelium of littermate control mice presents membrane-bound tomato red (*red*). *Scale bar*: 20 μm.

Importance of the Sulfation Pattern for Corneal Wound Healing

Studies have shown that the sulfation pattern of HS dictates its physiological function. *Ndst1* (*N*-deacetylase/*N*-sulfotransferase) converts GlcNHAc to $GlcNSO_3$ residues.[25,26] *Ndst* is considered by many to be the gateway enzyme since it is the enzyme that initiates the downstream HS chain modifications. Therefore, in order to elucidate whether the specific sulfation pattern is responsible for the epithelial defect associated with the knockout of *Ext1*, a mouse model was generated to knock out *Ndst1* instead of *Ext1*. The *NDST*$^{\Delta/\Delta CEpi}$ mice presented a decrease in the number of epithelial cell layers; however, the mice did not reproduce the extent of corneal defects associated with the *Ext1* gene (Fig. 9). Therefore, the less severe phenotype obtained with *NDST1*$^{\Delta/\Delta CEpi}$ mice could suggest that modifying the sulfation pattern alone was not enough to disrupt cell–cell adhesion complexes; however, other *Ndst* isoforms could have compensated for the loss of *Ndst1*, a possibility that is beyond the scope of this study.

Knockout of HS Leads to Increased Cell Proliferation

Our results suggest that the lack of HS disrupts cell–cell adhesions, leading to impaired stratification and increased sloughing off of cells, resulting in a drastic reduction in the number of epithelial cell layers. However, a significant decrease in cell proliferation could also contribute toward the observed phenotype. Therefore, cell proliferation was evaluated by Ki67 staining in *EXT*$^{\Delta/\Delta CEpi}$ mice and EdU incorporation in wounded and unwounded *EXT*$^{\Delta/\Delta CEpi}$ and *NDST*$^{\Delta/\Delta CEpi}$ mice. Cell proliferation by Ki67 staining was evaluated by whole-mount analysis of unwounded corneas, revealing an at least 6-fold increase in cell proliferation in *EXT*$^{\Delta/\Delta CEpi}$ mice when compared to the littermate control

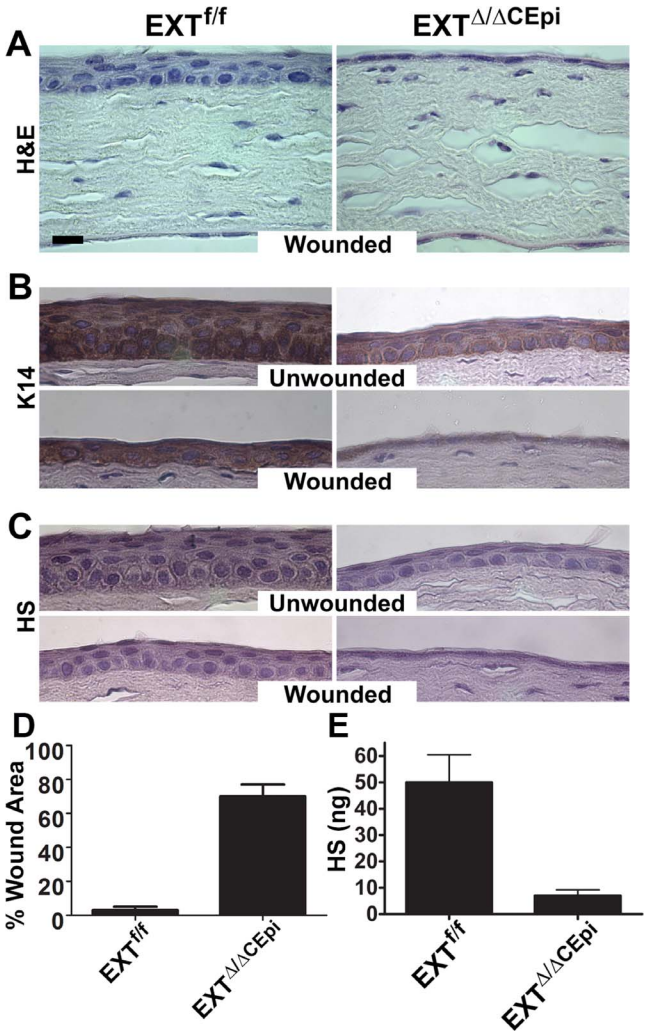

Figure 6. Wound healing of *EXT*$^{f/f}$ and *EXT*$^{\Delta/\Delta CEpi}$ mice. Debridement wounds were performed on P55 *EXT*$^{f/f}$ and *EXT*$^{\Delta/\Delta CEpi}$ mice induced from P21. The corneas were analyzed after 24 hours. *EXT*$^{\Delta/\Delta CEpi}$ mice presented compromised wound healing. Corneas were processed for paraffin sectioning and analyzed by (**A**) hematoxylin and eosin staining, (**B**) Krt14 staining, and (**C**) heparan sulfate staining of the wounded and unwounded contralateral cornea. (**D**) Percentage of wound area remaining 24 hours after wounding. The corneas of *EXT*$^{f/f}$ mice healed within 24 hours; however, *EXT*$^{\Delta/\Delta CEpi}$ mice had approximately 70% of the wound area remaining 24 hours after wounding. (**E**) GAGs were extracted from the corneas of *EXT*$^{f/f}$ and *EXT*$^{\Delta/\Delta CEpi}$ mice induced from P21 to P55 and chondroitin sulfate (CS) and dermatan sulfate (DS) was digested by chondroitinase ABC digestion. HS levels were assayed using the carbazole colorimetric assay, revealing a loss of HS expression in the corneas of *EXT*$^{\Delta/\Delta CEpi}$ mice when compared to littermate control mice (*EXT*$^{f/f}$). *Scale bar*: 20 μm.

mice (Fig. 10A). Cell proliferation by EdU incorporation was performed 7 days after debridement wounds, and wounded and unwounded corneas were analyzed by paraffin sectioning. Interestingly, we found an approximately 3-fold increase in *EXT*$^{\Delta/\Delta CEpi}$ corneal epithelial cell proliferation when compared to the littermate controls (Figs. 10B, 10C). Moreover, upon wounding, the *EXT*$^{\Delta/\Delta CEpi}$ corneal epithelial cells also presented a 2-fold increase in cell proliferation when compared to littermate controls, thereby suggesting that the observed phenotype is not a result of a decrease in cell proliferation (Figs. 10B, 10C). An approximately 2-fold increase was

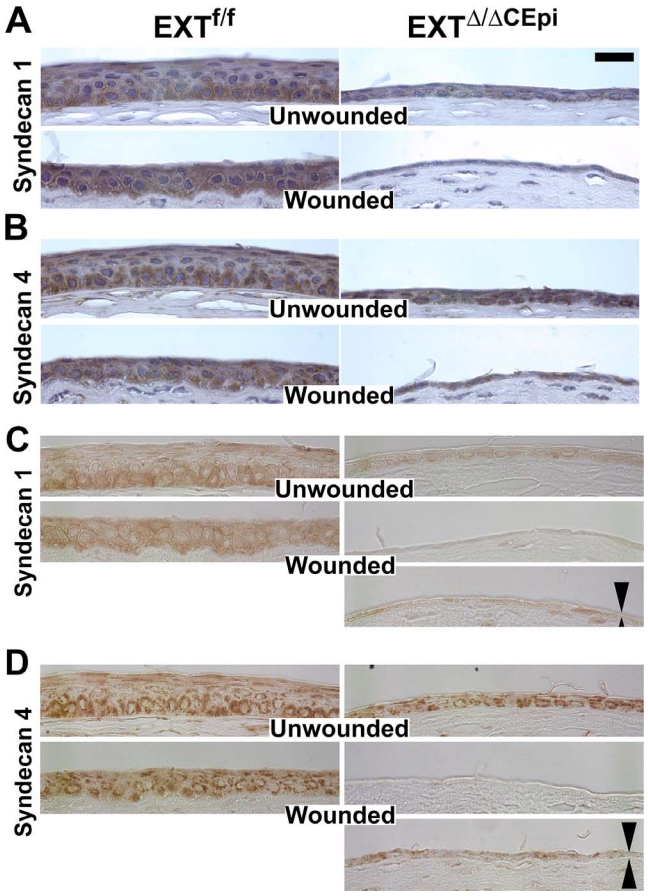

Figure 7. Syndecan-1 and -4 staining during corneal wound healing of $EXT^{f/f}$ and $EXT^{\Delta/\Delta CEpi}$ mice. Debridement wounds were performed on P55 $EXT^{f/f}$ and $EXT^{\Delta/\Delta CEpi}$ mice induced at P21 and analyzed after 24 hours. Corneas were processed for paraffin sectioning and analyzed for (**A**) syndecan-1 and (**B**) syndecan-4 with hematoxylin counterstain. (**C**, **D**) Syndecan-1 and -4 expression was also analyzed without the hematoxylin counterstain. (**C**) Syndecan-1 and (**D**) syndecan-4 can be observed in the unwounded corneas and both in the center of the wounded area and the wound edge of the wounded corneas (*double arrows*). Absence of hematoxylin counterstain enables a clearer visualization of DAB staining. *Scale bar*: 20 μm.

observed in the proliferation of $NDST^{\Delta/\Delta CEpi}$ mice when compared to littermate controls.

Discussion

Previous studies have shown that syndecan-1 and perlecan-deficient mice present impaired wound healing; however, the precise role played by the HS side chains was not demonstrated.[27,28] The GAG side chains play a vital role in the physiological function of proteoglycans. Recently, the Sulf 1 and 2 knockout mice were shown to display a similar phenotype to the syndecan-1 knockout mice presenting compromised wound healing.[29] However, the full extent of the importance of HS chains in corneal wound healing remains elusive. The knockout of *Ext1* in neural crest cells using the *Wnt1-Cre* conditional knockout system leads to ocular anterior segment dysgenesis; however, the mutant mice die within the first day of life, hindering further wound healing studies. Therefore, we generated a conditional inducible knockout mouse line to excise *Ext1* and *Ndst1* in the corneal epithelium of adult mice in order to elucidate the role of HS in corneal

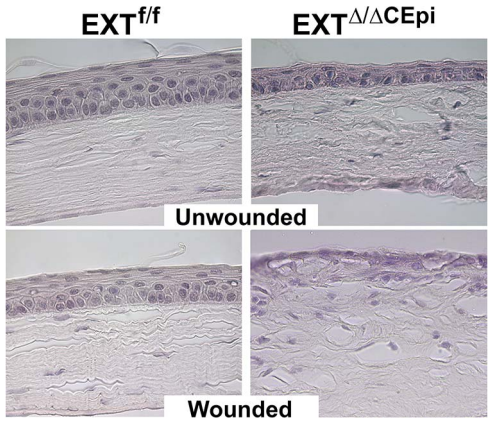

Figure 8. Failure to form a stratified epithelium 7 days after wounding in $EXT^{\Delta/\Delta CEpi}$ mice. Debridement wounds were performed on P55 $EXT^{f/f}$ and $EXT^{\Delta/\Delta CEpi}$ mice induced at P21 and analyzed after 7 days. $EXT^{\Delta/\Delta CEpi}$ mice presented compromised wound healing, persistent inflammation, and failure to form a stratified epithelium 7 days after wounding. Corneas were processed for paraffin sectioning and analyzed by hematoxylin and eosin staining.

homeostasis and wound healing. Interestingly, the corneal phenotype with ablation of HS in the corneal epithelium is more severe than with knocking out syndecan-1 or perlecan, which are major HSPGs expressed in the corneal epithelium and basement membrane, respectively; this is a testament to the importance of the GAG side chains in proteoglycan function.

Our studies demonstrate that HS is vital for maintaining corneal homeostasis. Mice lacking HS in the corneal epithelium presented significantly thinner corneas than littermate control mice, which became thinner with time after induction. When mice were induced from P21 to 120, $EXT^{\Delta/\Delta CEpi}$ mice presented corneas with solely two to four epithelial cell layers, and all cells presented compromised morphology. Our results show that the loss of cell layers is not due to decreased proliferation but to the loss of cell–cell adhesion, which leads to excessive sloughing off of epithelial cells. Syndecan-$1^{-/-}$ mice display corneal hypoplasia solely upon wounding and

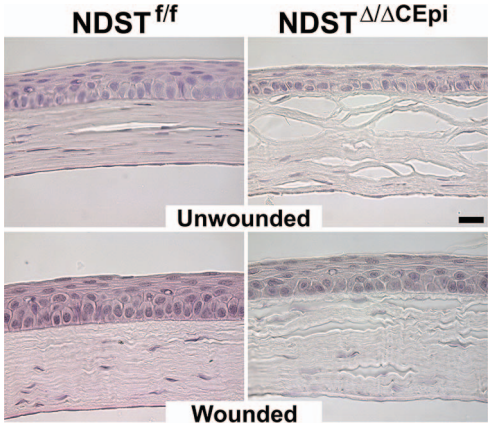

Figure 9. A stratified epithelium is formed 7 days after wounding in $NDST^{\Delta/\Delta CEpi}$ mice. Debridement wounds were performed on P55 $NDST^{f/f}$ and $NDST^{\Delta/\Delta CEpi}$ mice induced at P21 and analyzed after 7 days. $NDST^{\Delta/\Delta CEpi}$ mice presented compromised wound healing and thinner corneas 7 days after wounding when compared to $NDST^{f/f}$; however, it was not as severe as that observed for $EXT^{\Delta/\Delta CEpi}$ mice. Corneas were processed for paraffin sectioning and analyzed by hematoxylin and eosin staining. *Scale bar*: 20 μm.

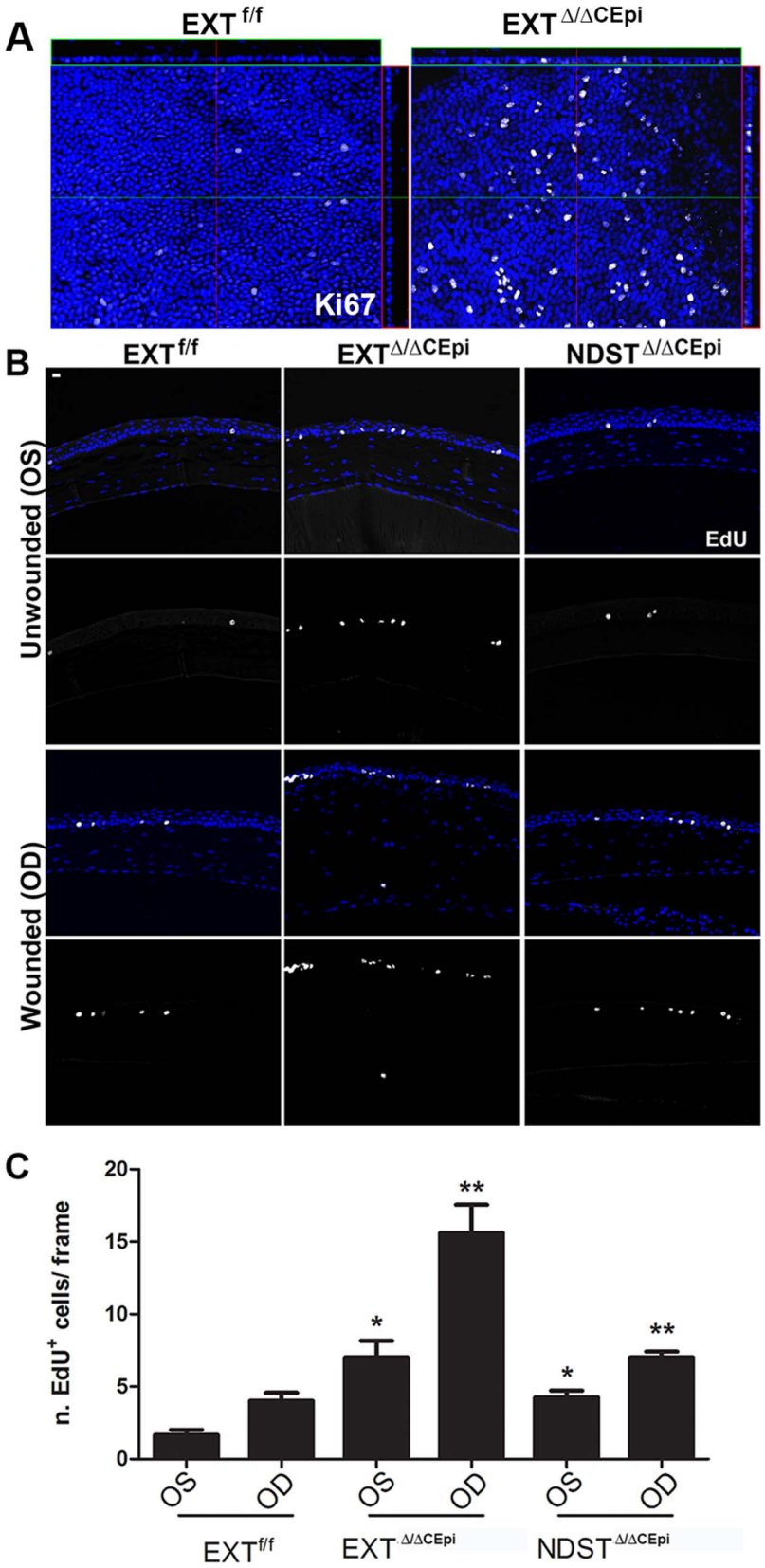

Figure 10. *EXT*$^{\Delta/\Delta CEpi}$ mice present increased cell proliferation. (**A**) Ki67 staining was performed on whole-mount corneas of P55 *EXT*$^{f/f}$ and *EXT*$^{\Delta/\Delta CEpi}$ mice induced at P21. (**B**) Debridement wounds were performed on P55 *EXT*$^{f/f}$, *EXT*$^{\Delta/\Delta CEpi}$, and *NDST*$^{\Delta/\Delta CEpi}$ mice induced at P21 and mice submitted to EdU labeling 7 days after wounding for 4 hours. *EXT*$^{\Delta/\Delta CEpi}$ mice presented an increase in EdU incorporation in both the wounded and unwounded corneas. Corneas were processed for paraffin sectioning and analyzed by Click-IT Assay using Alexa 647. EdU labeling of sections 7 days after wounding (OD) *EXT*$^{f/f}$, *EXT*$^{\Delta/\Delta CEpi}$, and *NDST*$^{\Delta/\Delta CEpi}$ mice compared to unwounded contralateral corneas (ES). (**C**) Number of EdU-positive cells in wounded and unwounded corneas of *EXT*$^{f/f}$, *EXT*$^{\Delta/\Delta CEpi}$, and *NDST*$^{\Delta/\Delta CEpi}$ mice. *Scale bar*: 20 μm.

Investigative Ophthalmology & Visual Science

also show delayed wound healing[28]—a similar phenotype to the results obtained with the *NDST*$^{\Delta/\Delta CEpi}$ mice. However, neither *EXT*$^{\Delta/\Delta CEpi}$ mice nor *NDST*$^{\Delta/\Delta CEpi}$ mice presented reduced cell proliferation upon wounding as reported for syndecan 1$^{-/-}$ and perlecan$^{-/-}$ (Hspg2$^{-/-Tg}$) mice.[28] Moreover, syndecan-1$^{-/-}$ mice did not display compromised barrier function.[28] Perlecan$^{-/-}$ (Hspg2$^{-/-Tg}$) mice also display a progressive decrease in epithelial cell layers, which is consistent with our data.[27]

Corneal wound healing is a complex process that involves precise regulation of clotting, inflammatory cell infiltration, prevention of angiogenesis, and re-epithelialization. Recently a synergic role has been shown between syndecans and integrins that is essential for cell migration.[30,31] The expression of both integrins and syndecans is tightly modulated during wound healing, and mainly regulated by growth factors and/or exposure to the ECM.[32–36] In uninjured mouse skin, syndecan-4 is expressed solely by epidermal cells; however, following injury, expression is upregulated throughout the dermis[37] and impaired wound healing is the major phenotype of syndecan-4$^{-/-}$ mice. Moreover, fibroblasts isolated from syndecan 4$^{-/-}$ mice display reduced wound healing in vitro.[38]

Syndecan-1 has a well-established role in the wound healing response. Syndecan-1 expression is restricted to the epithelium of normal mouse tissue and is upregulated in dermal endothelial cells and granulation tissue fibroblasts during tissue repair. This switch in expression mirrors the change in syndecan-1 expression that occurs during embryonic epithelial cell morphogenesis, when expression of syndecan-1 becomes reduced in the epithelium and elevated in associated mesenchymal cells. After protease- or growth factor-mediated shedding, the syndecan-1 ectodomain accumulates in wounds. Therefore, both syndecan-1 and syndecan-4 are involved in dermal wound healing; however, syndecan-1 seems to be primarily involved in keratinocyte function and re-epithelialization, while syndecan-4 seems to be primarily associated with fibroblast migration, wound contraction, and angiogenesis. Although studies have demonstrated the role of HSPGs in wound healing, the role of the HS side chains remains to be elucidated.

Further indication of the important role of HS in corneal wound healing is the finding that knocking out Sulf 1 and Sulf 2, both in vivo and in vitro, leads to compromised corneal wound healing.[29] The binding of ligands to HS chains is dictated by the pattern of four sulfate modifications. Sulf 1 and Sulf 2 are secreted endosulfatases that remove the 6-O sulfation from glucosamine (6OS) within the ECM. Thus the expression of Sulfs directly modulates the binding of growth factors to HS chains.[13,39–44] Maltseva et al.[29] showed that specifically the removal of 6-O sulfation hindered the Wnt/β-catenin signaling pathway upon corneal wounding. However, to date no study has evaluated the full extent of the role of HS chains in corneal wound healing.

Our study reveals that mice lacking HS in the corneal epithelium present drastically compromised wound healing. The absence of HS hinders the formation of a stratified epithelium upon wounding, and the delayed corneal resurfacing of epithelial cells after wounding leads to stromal damage. However, *NDST*$^{\Delta/\Delta CEpi}$ mice present a more subtle phenotype resembling that observed for Sulf 1, Sulf 2, and syndecan-1 knockout mice. *EXT*$^{\Delta/\Delta CEpi}$ and *NDST*$^{\Delta/\Delta CEpi}$ mice presented increased proliferation and *EXT*$^{\Delta/\Delta CEpi}$ mice presented compromised cell–cell adhesion, which leads to the premature sloughing off of epithelial cells. Moreover, the decrease in Krt12 staining in *EXT*$^{\Delta/\Delta CEpi}$ mouse epithelial cells suggests that there is compromised differentiation of epithelial cells, which is consistent with compromised stratification. The loss of tight junctions and/or an increased proliferation and upward growth could jeopardize the differentiation of epithelial cells.

It is of interest to note that a mouse model was generated to ablate HS expression in the corneal stroma using the keratocan-inducible promoter, thereby generating the mouse model *EXT*$^{\Delta/\Delta CStr}$. In this mouse model the keratocytes lacked HS side chains; however, the other corneal structures retained normal HS expression. Interestingly, these mice presented no macroscopic or microscopic corneal defects and no significant differences upon wounding using both debridement wounds and alkali burn (data not shown). These data suggest that HS expression is essential for the maintenance of corneal homeostasis in the epithelium, but does not play a vital role in maintaining homeostasis of the stroma.

Taken together, our findings clearly show that HS is essential for maintaining integrity of the corneal epithelium. Moreover, the loss of epithelial HS hinders corneal wound healing and corneal epithelial stratification. The severity of the epithelial phenotype associated with the knockout of HS when compared to that observed in the syndecan-1 and perlecan knockout mouse lines indicates the vital role HS plays in corneal wound healing. Follow-up studies with syndecan-4 and compound knockout mouse models (syndecan-1$^{-/-}$ and Hspg2$^{-/-Tg}$) mice could shed light on the vital role HSPGs play in maintaining corneal integrity. Interestingly, the ablation of HS in corneal keratocytes caused no significant damage and did not impair wound healing.

Acknowledgments

The authors thank Tarsis F. Gesteira, PhD, and Mindy Call, PhD, for all their valuable help throughout the study.

Supported by National Institutes of Health/National Eye Institute Grants RO1 EY011845 and EY021798, Research to Prevent Blindness, and Ohio Lions Eye Research Foundation.

Disclosure: **V.J. Coulson-Thomas**, None; **S.-H. Chang**, None; **L.-K. Yeh**, None; **Y.M. Coulson-Thomas**, None; **Y. Yamaguchi**, None; **J. Esko**, None; **C.-Y. Liu**, None; **W. Kao**, None

References

1. Gesteira TF, Coulson-Thomas VJ, Ogata FT, et al. A novel approach for the characterisation of proteoglycans and biosynthetic enzymes in a snail model. *Biochim Biophys Acta*. 2011;1814:1862–1869.
2. Bishop JR, Schuksz M, Esko JD. Heparan sulphate proteoglycans fine-tune mammalian physiology. *Nature*. 2007;446:1030–1037.
3. Meyers JR, Planamento J, Ebrom P, Krulewitz N, Wade E, Pownall ME. Sulf1 modulates BMP signaling and is required for somite morphogenesis and development of the horizontal myoseptum. *Dev Biol*. 2013;378:107–121.
4. Bush KT, Crawford BE, Garner OB, Nigam KB, Esko JD, Nigam SK. N-sulfation of heparan sulfate regulates early branching events in the developing mammary gland. *J Biol Chem*. 2012;287:42064–42070.
5. Shah MM, Sakurai H, Gallegos TF, et al. Growth factor-dependent branching of the ureteric bud is modulated by selective 6-O sulfation of heparan sulfate. *Dev Biol*. 2011;356:19–27.
6. Qu X, Carbe C, Tao C, et al. Lacrimal gland development and Fgf10-Fgfr2b signaling are controlled by 2-O- and 6-O-sulfated heparan sulfate. *J Biol Chem*. 2011;286:14435–14444.
7. Delehedde M, Lyon M, Sergeant N, Rahmoune H, Fernig DG. Proteoglycans: pericellular and cell surface multireceptors that integrate external stimuli in the mammary gland. *J Mammary Gland Biol Neoplasia*. 2001;6:253–273.

8. Lander AD, Nie Q, Wan FY. Do morphogen gradients arise by diffusion? *Dev Cell*. 2002;2:785–796.
9. Zieske JD. Extracellular matrix and wound healing. *Curr Opin Ophthalmol*. 2001;12:237–241.
10. Saika S, Ohnishi Y, Ooshima A, Liu CY, Kao WW. Epithelial repair: roles of extracellular matrix. *Cornea*. 2002;21:S23–S29.
11. Wilson SE, Mohan RR, Ambrosio R, Mohan RR. Corneal injury. A relatively pure model of stromal-epithelial interactions in wound healing. *Methods Mol Med*. 2003;78:67–81.
12. Yamanaka O, Yuan Y, Coulson-Thomas VJ, et al. Lumican binds ALK5 to promote epithelium wound healing. *PLoS One*. 2013; 8:e82730.
13. Yue X, Lu J, Auduong L, Sides MD, Lasky JA. Overexpression of Sulf2 in idiopathic pulmonary fibrosis. *Glycobiology*. 2013;23: 709–719.
14. Nguyen H, Rendl M, Fuchs E. Tcf3 governs stem cell features and represses cell fate determination in skin. *Cell*. 2006;127: 171–183.
15. Perl AK, Wert SE, Nagy A, Lobe CG, Whitsett JA. Early restriction of peripheral and proximal cell lineages during formation of the lung. *Proc Natl Acad Sci U S A*. 2002;99: 10482–10487.
16. Muzumdar MD, Tasic B, Miyamichi K, Li L, Luo L. A global double-fluorescent Cre reporter mouse. *Genesis*. 2007;45: 593–605.
17. Inatani M, Irie F, Plump AS, Tessier-Lavigne M, Yamaguchi Y. Mammalian brain morphogenesis and midline axon guidance require heparan sulfate. *Science*. 2003;302:1044–1046.
18. Grobe K, Inatani M, Pallerla SR, Castagnola J, Yamaguchi Y, Esko JD. Cerebral hypoplasia and craniofacial defects in mice lacking heparan sulfate Ndst1 gene function. *Development*. 2005;132:3777–3786.
19. Zhu G, Ishizaki M, Haseba T, Wu RL, Sun TT, Kao WW. Expression of K12 keratin in alkali-burned rabbit corneas. *Curr Eye Res*. 1992;11:875–887.
20. Moyer PD, Kaufman AH, Zhang Z, Kao CW, Spaulding AG, Kao WW. Conjunctival epithelial cells can resurface denuded cornea, but do not transdifferentiate to express cornea-specific keratin 12 following removal of limbal epithelium in mouse. *Differentiation*. 1996;60:31–38.
21. Nelson WG, Sun TT. The 50- and 58-kdalton keratin classes as molecular markers for stratified squamous epithelia: cell culture studies. *J Cell Biol*. 1983;97:244–251.
22. Byrne C, Tainsky M, Fuchs E. Programming gene expression in developing epidermis. *Development*. 1994;120:2369–2383.
23. Cenedella RJ, Fleschner CR. Kinetics of corneal epithelium turnover in vivo. Studies of lovastatin. *Invest Ophthalmol Vis Sci*. 1990;31:1957–1962.
24. Coulson-Thomas VJ, Gesteira TF, Esko J, Kao W. Heparan sulfate regulates hair follicle and sebaceous gland morphogenesis and homeostasis. *J Biol Chem*. 2014;289:25211–25226.
25. Gesteira TF, Coulson-Thomas VJ, Taunay-Rodrigues A, et al. Inhibitory peptides of the sulfotransferase domain of the heparan sulfate enzyme, N-deacetylase-N-sulfotransferase-1. *J Biol Chem*. 2011;286:5338–5346.
26. Gesteira TF, Pol-Fachin L, Coulson-Thomas VJ, Lima MA, Verli H, Nader HB. Insights into the N-sulfation mechanism: molecular dynamics simulations of the N-sulfotransferase domain of NDST1 and mutants. *PLoS One*. 2013;8:e70880.
27. Inomata T, Ebihara N, Funaki T, et al. Perlecan-deficient mutation impairs corneal epithelial structure. *Invest Ophthalmol Vis Sci*. 2012;53:1277–1284.
28. Stepp MA, Gibson HE, Gala PH, et al. Defects in keratinocyte activation during wound healing in the syndecan-1-deficient mouse. *J Cell Sci*. 2002;115:4517–4531.
29. Maltseva I, Chan M, Kalus I, Dierks T, Rosen SD. The SULFs, extracellular sulfatases for heparan sulfate, promote the migration of corneal epithelial cells during wound repair. *PLoS One*. 2013;8:e69642.
30. Han J, Lim CJ, Watanabe N, et al. Reconstructing and deconstructing agonist-induced activation of integrin alphaIIb-beta3. *Curr Biol*. 2006;16:1796–1806.
31. Morgan MR, Humphries MJ, Bass MD. Synergistic control of cell adhesion by integrins and syndecans. *Nat Rev Mol Cell Biol*. 2007;8:957–969.
32. Hertle MD, Kubler MD, Leigh IM, Watt FM. Aberrant integrin expression during epidermal wound healing and in psoriatic epidermis. *J Clin Invest*. 1992;89:1892–1901.
33. Cavani A, Zambruno G, Marconi A, Manca V, Marchetti M, Giannetti A. Distinctive integrin expression in the newly forming epidermis during wound healing in humans. *J Invest Dermatol*. 1993;101:600–604.
34. Christofidou-Solomidou M, Bridges M, Murphy GF, Albelda SM, DeLisser HM. Expression and function of endothelial cell alpha v integrin receptors in wound-induced human angiogenesis in human skin/SCID mice chimeras. *Am J Pathol*. 1997;151:975–983.
35. Reynolds LE, Conti FJ, Lucas M, et al. Accelerated re-epithelialization in beta3-integrin-deficient- mice is associated with enhanced TGF-beta1 signaling. *Nat Med*. 2005;11:167–174.
36. Zambruno G, Marchisio PC, Marconi A, et al. Transforming growth factor-beta 1 modulates beta 1 and beta 5 integrin receptors and induces the de novo expression of the alpha v beta 6 heterodimer in normal human keratinocytes: implications for wound healing. *J Cell Biol*. 1995;129:853–865.
37. Gallo R, Kim C, Kokenyesi R, Adzick NS, Bernfield M. Syndecans-1 and -4 are induced during wound repair of neonatal but not fetal skin. *J Invest Dermatol*. 1996;107:676–683.
38. Echtermeyer F, Streit M, Wilcox-Adelman S, et al. Delayed wound repair and impaired angiogenesis in mice lacking syndecan-4. *J Clin Invest*. 2001;107:R9–R14.
39. Ai X, Do AT, Lozynska O, Kusche-Gullberg M, Lindahl U, Emerson CP Jr. QSulf1 remodels the 6-O sulfation states of cell surface heparan sulfate proteoglycans to promote Wnt signaling. *J Cell Biol*. 2003;162:341–351.
40. Viviano BL, Paine-Saunders S, Gasiunas N, Gallagher J, Saunders S. Domain-specific modification of heparan sulfate by Qsulf1 modulates the binding of the bone morphogenetic protein antagonist Noggin. *J Biol Chem*. 2004;279:5604–5611.
41. Wang S, Ai X, Freeman SD, et al. QSulf1, a heparan sulfate 6-O-endosulfatase, inhibits fibroblast growth factor signaling in mesoderm induction and angiogenesis. *Proc Natl Acad Sci U S A*. 2004;101:4833–4838.
42. Ai X, Kitazawa T, Do AT, Kusche-Gullberg M, Labosky PA, Emerson CP Jr. SULF1 and SULF2 regulate heparan sulfate-mediated GDNF signaling for esophageal innervation. *Development*. 2007;134:3327–3338.
43. Lemjabbar-Alaoui H, van Zante A, Singer MS, et al. Sulf-2, a heparan sulfate endosulfatase, promotes human lung carcinogenesis. *Oncogene*. 2010;29:635–646.
44. Phillips JJ, Huillard E, Robinson AE, et al. Heparan sulfate sulfatase SULF2 regulates PDGFRα signaling and growth in human and mouse malignant glioma. *J Clin Invest*. 2012;122: 911–922.

Investigative Ophthalmology & Visual Science